NMR Characterization of the Metallo-β-lactamase from *Bacteroides fragilis* and Its Interaction with a Tight-Binding Inhibitor: Role of an Active-Site Loop†

Sergio D. B. Scrofani,‡,§ John Chung,‡ James J. A. Huntley,‡ Stephen J. Benkovic,|| Peter E. Wright,‡ and H. Jane Dyson*,‡

Department of Molecular Biology and Skaggs Institute of Chemical Biology, The Scripps Research Institute, 10550 North Torrey Pines Road, La Jolla, California 92037, and Department of Chemistry, The Pennsylvania State University, University Park, Pennsylvania 16802

Received April 29, 1999; Revised Manuscript Received July 28, 1999

ABSTRACT: Understanding the structure and dynamics of the enzymes that mediate antibiotic resistance of pathogenic bacteria will allow us to take steps to combat this increasingly serious public health hazard. Complete backbone NMR resonance assignments have been made for the broad-specificity metallo-β-lactamase CcrA from *Bacteroides fragilis* in the presence and absence of a tight-binding inhibitor. Chemical shift indices show that the secondary structure of the CcrA molecule in solution is very similar to that in published crystal structures. A loop adjacent to the two-zinc catalytic site exhibits significant structural variation in the published structures, but appears from the NMR experiments to be a regular β-hairpin. Backbone heteronuclear NOE measurements indicate that this region has slightly greater flexibility on a picosecond to nanosecond time scale than the molecule as a whole. The loop appears to have an important role in the binding of substrates and inhibitors. Binding of the inhibitor 3-[2′-(*S*)-benzyl-3′-mercaptopropanoyl]-4-(*S*)-carboxy-5,5-dimethylthiazolidine causes a marked increase in the stability of the protein toward unfolding and aggregation, and causes changes in the NMR resonance frequencies of residues close to the active (zinc-binding) site, including the β-hairpin loop. There is a small but significant increase in the heteronuclear NOE for this loop upon inhibitor binding, indicative of a decrease in flexibility. In particular, the NOE of the indole ring of tryptophan 49, at the tip of the β-hairpin loop, changes from a low value characteristic of a random coil chain to a significantly higher value, close to that observed for the backbone amides in this region of the protein. These results strongly suggest that the hairpin loop participates in the binding of substrate and in the shielding of the zinc sites from solvent. The broad specificity of the CcrA metallo-β-lactamase may in fact reside in the plasticity of this part of the protein, which allows it to accommodate and bind tightly to substrates of a variety of shapes and sizes.

In the 1980s, it was widely believed that the era of bacterial infections had largely passed. However, the 1990s saw a worldwide resurgence with the advent of pathogenic bacteria resistant to multiple antibiotics (*1*). Subsequent investigations suggested that the heavy use of antibacterial drugs in hospitals and in agriculture had become an evolutionary force, selecting and enhancing the survival of bacterial strains that could resist them. One of the most important groups of enzymes implicated in antibiotic resistance are the β-lactamases, which hydrolyze the four-membered ring C−N bond of penicillin and cephalosporin antibiotics, giving a product that no longer inhibits a transpeptidase necessary for bacterial cell wall synthesis (*2*). Four major classes of β-lactamases have been identified on the basis of sequence similarities (*3*). Groups 1, 2, and 4, differing only in interactions with substrates and inhibitors, are serine hydrolases that catalyze the hydrolysis of β-lactams by a double-displacement mechanism involving an acyl−enzyme intermediate (*2*). Phosphonate and sulbactam compounds, such as clavulanic acid (*4*), are potent inhibitors of these enzymes. However, group 3 β-lactamases, which require metal ions for activity, exhibit broad spectrum resistance to all clinically effective inhibitors. A series of mercaptoacetic acid thiol ester derivatives have been found to inhibit metallo-β-lactamases from some, but not all, organisms (*5*). The appearance of plasmid-mediated metallo-β-lactamases (*6*, *7*) has made the rapid dissemination of metallo-β-lactamase resistance in pathogens a distinct and frightening possibility (*8*). Consequently, effective inhibitors which counter metallo-β-lactamase activity are required.

Bacteroides fragilis has been termed one of the most important anaerobic bacterial pathogens of humans (*9*), and antibiotic resistance is manifest through the production of metallo-β-lactamase which appears to be unaffected in the clinic by all β-lactamase inhibitors developed so far. The metallo-β-lactamase from *B. fragilis* (CcrA)[1] possesses a binuclear zinc site and has a molecular mass of approximately

† This work was supported by Grant GM 56879 from the National Institutes of Health. S.D.B.S. was a recipient of a Fulbright Postdoctoral Fellowship.

* To whom correspondence should be addressed: Department of Molecular Biology MB2, The Scripps Research Institute, 10550 N. Torrey Pines Rd., La Jolla, CA 92037.

‡ The Scripps Research Institute.

§ Present address: AMRAD Operations, Private Box 29, Richmond, Victoria 3121, Australia.

|| The Pennsylvania State University.

10.1021/bi990986t CCC: $18.00
Published on Web 10/14/1999

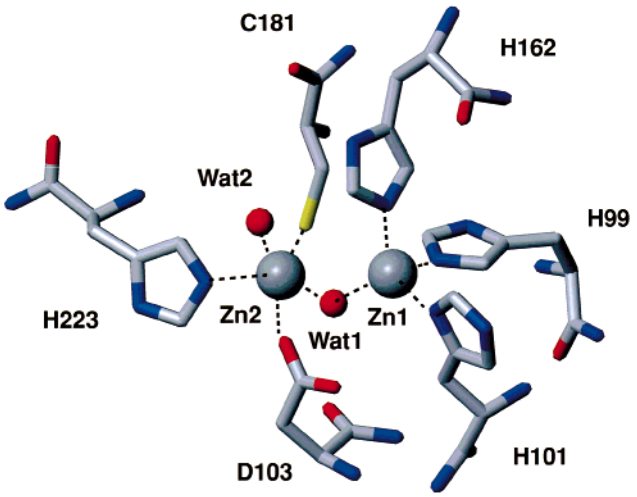

FIGURE 1: Coordination environment of the zinc sites in the *B. fragilis* metallo-β-lactamase (*11*), showing the bridging water (Wat 1) and the water (Wat 2) coordinated to Zn2.

27 kDa (249 amino acids), where amino acids 1−17 form a propeptide that is not present in the mature enzyme. Cobalt(II) substitution and site-directed mutagenesis studies indicate that the enzyme binds each metal ion with micromolar affinity (*10*).

A crystal structure of the enzyme has been determined to 1.85 Å resolution (*11*); the molecule exhibits an $\alpha\beta\beta\alpha$ structure motif. The metal ions are bridged by a common water/hydroxide molecule, and additional ligands to each zinc ion include three histidines (His99, His101, and His162) to the first zinc ion (Zn1), and a cysteine thiolate (Cys181), an aspartate carboxyl group (Asp103), a histidine (His223), and an additional water molecule to the second site, Zn2 (*11*) (Figure 1). One feature of this structure is the presence of a loop close to the zinc binding site, which exhibited high temperature factors for part of its length; no density was observed for two of the residues, Gly48 and Trp49. Although later crystal structures have been able to localize this density (*12*, *13*), this loop is highly variable between structures, and its structure appears to be stabilized by crystal packing in almost all cases where it is observable. This paper addresses the conformational variability of this loop in solution and, via examination of the changes in the NMR spectrum of the protein in the presence and absence of a tight-binding inhibitor, explores the function of the loop in the enzyme.

MATERIALS AND METHODS

Sample Preparation. The protein was prepared by methods similar to those recently described (*10*) with the following modifications for high-yield growth on labeled media and for extremely pure NMR samples. The plasmid pT7CcrANDE02 (*14*) was transformed into *Escherichia coli* BL21(DE3) cells, and metallo-β-lactamase CcrA was overexpressed in minimal medium consisting of a modified form of the preparation described by Neidhardt et al. (*15*), supplemented with basal Eagle vitamin supplement (BRL) and kanamycin (1 mL of a 25 mg/mL solution per liter). For ^{15}N-labeled CcrA, the growth medium was supplemented with $^{15}NH_4Cl$ (1 g/L) as the sole nitrogen source. For the uniformly ^{13}C- and ^{15}N-labeled enzyme, the same medium was used with the exception being that [^{13}C]glucose (2 g/L) was the sole carbon source. A 40 mL culture grown overnight at 30 °C (OD_{550} ∼ 1.6) was used to inoculate 1 L of Neidhardt medium. Cultures were grown at 30 °C to OD_{550} of ∼0.6−0.7 and induced with 1.0 mM IPTG followed by addition of 100 μM $ZnSO_4$. Cultures were allowed to grow for one doubling time (2 h) before being harvested. Wet cell yields were typically 1.8−1.9 g/L. For ^{2}H-, ^{13}C-, and ^{15}N-labeled CcrA, the cells were grown as described previously, with the exception being that ^2H_2O (99.8%) and sodium [$^{13}C_2$]acetate (2 g/L) replaced the water and carbon sources, respectively. Due to differences in their metabolic pathways, the use of sodium acetate as the sole carbon source allows a more random level of deuteration than is possible with glucose (*16*). The pH of the deuterated medium was corrected for isotope effects to pD 7.4 (*17*). The inoculum was grown in Neidhardt medium prepared with 50% ^2H_2O and grown for 64 h (OD_{550} ∼ 1.4). Four 1 L cultures in 99.8% ^2H_2O were each inoculated with 30 mL of inoculum and grown for 45 h to an OD_{550} of ∼0.65. After induction with 1 mM IPTG and addition of 1 mM $ZnSO_4$, cells were grown for an additional 10 h (one doubling time) and harvested. In contrast to cultures grown in a fully protonated medium, no increase in cell density was observed after induction. Final cell yields were 0.8 g/L, approximately half the yield obtained when cells were grown in H_2O with sodium acetate as the sole carbon source. All cells were stored at −70 °C until they were required.

Cells were suspended in 9 mL of buffer A [10 mM HEPES and 100 μM $ZnSO_4$ (pH 7.2)] per liter of culture and allowed to stand at room temperature for at least 1 h. Cell lysis, which includes incubations with DNAse, was achieved by using previously described methods (*18*). Lysed cells were sonicated for 6 × 1 min to ensure complete cell disruption, and the suspension was centrifuged at 16 000 rpm for 20 min. The inclusion bodies containing the CcrA were washed with buffer A and centrifuged (16 000 rpm for 20 min) twice, followed by resuspension in 0.5 mL of buffer A. Once the inclusion bodies had been thoroughly resuspended, 9 mL of 8 M urea, 10 mM HEPES, 100 μM $ZnSO_4$, and 10 mM DTT (pH 7.6) was added per liter of culture. Following brief sonication, the solution was allowed to stand at room temperature for at least 1 h, after which it was centrifuged (16 000 rpm for 20 min) to remove undissolved matter. The clarified solution was then transferred to dialysis tubing (12 kDa cutoff; Spectrapor) and dialyzed overnight against 2 L of 10 mM Tris-HCl, 10 mM DTT, and 100 μM $ZnCl_2$ (pH 7.2) and 4 °C, yielding a slightly turbid solution. Residual lipid and cell wall debris were removed with a Millex-GV filter (0.45 μM; Millipore). This solution was applied to a Pharmacia HiTrap Q column (5 mL) equilibrated in 50 mM Tris-HCl and 100 μM $ZnCl_2$ (pH 7.0) and washed until baseline absorbance was achieved. Metallo-β-lactamase was eluted from the column using 50 mM Tris-HCl, 1 M NaCl, and 100 μM $ZnCl_2$ (pH 7.0) at an NaCl concentration of

[1] Abbreviations: CcrA, protein (and gene) corresponding to the metallo-β-lactamase from *B. fragilis*; NMR, nuclear magnetic resonance; NOE, nuclear Overhauser effect; IPTG, isopropyl β-D-thiogalactoside; DTT, dithiothreitol; HEPES, *N*-(2-hydroxyethyl)piperazine-*N*′-2-ethanesulfonic acid; k_{cat}, rate of a catalyzed reaction; K_m, Michaelis constant; V_{max}, maximum reaction rate at high substrate concentrations; DSS, 2,2-(dimethylsilyl)propanesulfonic acid; CSI, chemical shift index; HSQC, homonuclear single-quantum coherence; EDTA, ethylenediaminetetraacetic acid; DMSO, dimethyl sulfoxide.

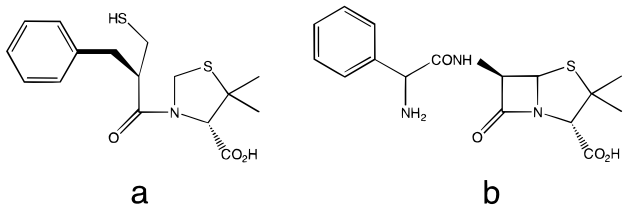

FIGURE 2: Structural comparison of (a) SB225666 and (b) ampicillin.

0.05−0.10 M. Fractions containing metallo-β-lactamase were pooled, diluted 2-fold, and reapplied to a fresh HiTrap Q column. The concentrated protein (6 mg/mL) was eluted from the column with 50 mM Tris-HCl, 100 μM $ZnCl_2$, and 0.45 M NaCl (pH 7.0) and dialyzed against 10 mM HEPES, 10 mM $ZnCl_2$, and 0.01% NaN_3 (pH 7.0) overnight. Samples were concentrated to 125 μM to 1.3 mM using an Amicon Centricon 10 ultrafilter (>90% recovery). Yields of purified enzyme were typically 15 mg/L of culture. No evidence for aggregation or dimerization was observed by gel filtration or SDS−PAGE for samples prepared in this manner. Metallo-β-lactamase preparations were assayed using nitrocefin (Oxoid) and yielded the following kinetic values: $k_{cat} = 214\ s^{-1}$, $K_m = 13.8\ \mu M$, and $V_{max} = 1.3\ \mu M\ s^{-1}$, consistent with published data (*19*).

Samples of the proprietary inhibitor 3-[2′-(*S*)-benzyl-3′-mercaptopropanoyl]-4-(*S*)-carboxy-5,5-dimethylthiazolidine (SB225666) (Figure 2) were obtained from SmithKline-Beecham. NMR samples of CcrA (125 μM to 1.3 mM) bound to SB225666 were prepared by the addition of the inhibitor dissolved in dimethyl sulfoxide (DMSO) under anaerobic conditions to a final concentration of 6 mM and 3% DMSO.

NMR Spectroscopy. A list of experiments performed on CcrA, together with the parameters used, is included in the Supporting Information. Spectra were acquired at 22 °C on Bruker AMX-500 and -600 and DRX-600 and -750 spectrometers, equipped with either 5 mm inverse-detected triple-resonance triple-axis gradient probes also from Bruker or 8 mm inverse-detected triple-resonance single-axis gradient probes from Nalorac (Martinez, CA). All triple-resonance experiments were performed with either uniformly ^{13}C- and ^{15}N-labeled or ^{2}H-, ^{13}C-, and ^{15}N-labeled CcrA in 95% H_2O and 5% $^{2}H_2O$. ^{15}N HSQC, ^{15}N TOCSY-HSQC, and ^{15}N NOESY-HSQC experiments were performed with CcrA uniformly labeled with ^{15}N.

All triple-resonance experiments were modified to include ^{15}N coherence selection via pulsed field gradients (*20*, *21*). Quadrature detection was achieved using either the States−TPPI method or gradient coherence selection with sensitivity enhancements in the indirect dimension (*20*). Water suppression in the ^{15}N HSQC, ^{15}N NOESY-HSQC, and ^{15}N TOCSY-HSQC experiments was achieved using a water flip-back pulse (*23*).

Heteronuclear NOE measurements were taken on low-concentration samples (125 and 250 μM) using the 8 mm probe, taking special precautions to minimize the intense water resonance in the presence of severe radiation damping and in the absence of the usual sensitivity enhancements afforded by any direct INEPT transfer polarization from ^{1}H to ^{15}N. Water flip-back pulses were not used.

Spectra were processed using either Felix 95.0 (MSI) or the NMRPipe (*24*) software package and analyzed with either Felix 95.0 or NMRView (*25*). Linear prediction was used to extend indirect dimensions, improving digital resolution. For experiments acquired with constant time in the ^{15}N dimension, mirror image linear prediction was utilized (*24*), allowing up to twice the number of data points to be predicted. Proton chemical shifts were referenced to external 2,2-(dimethylsilyl)propanesulfonic acid (DSS), and ^{15}N and ^{13}C chemical shifts were referenced indirectly to DSS (*26*).

RESULTS

Aggregation and Degradation of CcrA in the Presence of Phosphate. The anion exchange purification protocol described in this paper is the result of an extensive series of experiments, some of which have yielded insights into the nature of the active site of the metallo-β-lactamase. Extensive purification is necessary to remove high-molecular mass impurities apparently consisting of aggregated CcrA which has lost one or more zinc ions. A more subtle minor impurity appears to be a trace of plasmid DNA which remains even after the initial treatment of the cell lysate with DNAse. This impurity is removed by the anion exchange purification step, where it is eluted only at high salt concentrations (>0.5 M NaCl). Incubation of the high-salt fractions with DNAse and electrophoretic studies with ethidium bromide confirmed that this impurity consists of DNA. Its copurification with the metallo-β-lactamase in gel filtration steps must be ascribed either to a fortuitous similarity in molecular mass or to binding of the DNA to the protein.

If these impurities are not completely removed, the NMR samples show signs of time-dependent degradation. The high-molecular mass aggregates can be removed by gel filtration, but the resulting mixture containing the DNA impurity is found to bind to ultrafiltration membranes and so is difficult to concentrate. A procedure whereby samples were lyophilized and reconstituted at higher concentrations was moderately successful, but necessitated the use of phosphate buffer. Degradation products including aggregates were observed to form over a period of days to weeks. The extent of sample degradation appears to correlate with increased phosphate concentrations, and rapid degradation and aggregation were observed at phosphate concentrations of >80 mM. Since phosphate has a high affinity for zinc ions, it is likely that zinc is sequestered from the catalytic active sites to form insoluble $Zn_3(PO_4)_2$, suggesting that the removal of zinc ions from the active site precedes or accompanies aggregation. This is consistent with the observation that when the metal chelator EDTA is added to highly stable NMR samples prepared using the ion exchange protocol, aggregation occurs within hours (*27*). The stability and tendency of the protein to exist as a monomer are greatly improved in the presence of the inhibitor, presumably due to the lowered solvent accessibility of the zinc site.

Resonance Assignments and Secondary Structure of Free CcrA. The backbone resonance assignments of CcrA in the absence of inhibitor have been reported previously (*28*). The secondary structure elements of the solution structure of CcrA were evaluated using the chemical shift index method (CSI) of Wishart and Sykes (*29*), and compared to secondary structure elements predicted from the X-ray structure of CcrA (*11*) using the program PROCHECK (*30*) (Figure 3a). Locations of secondary structure elements derived from the

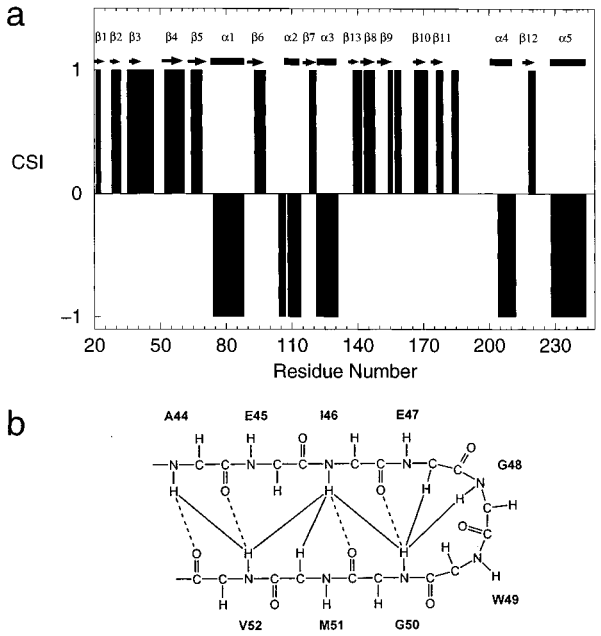

FIGURE 3: (a) Chemical shift index (*29*) as a function of residue number for the metallo-β-lactamase. The superimposed secondary structure elements are derived from the coordinates of the X-ray structure of CcrA (*11*). (b) β-Sheet schematic representation showing NOE connectivities (solid lines) that define the antiparallel β-sheet structure in the flexible loop region (residues 44−52). Dotted lines represent potential backbone−backbone hydrogen bonds.

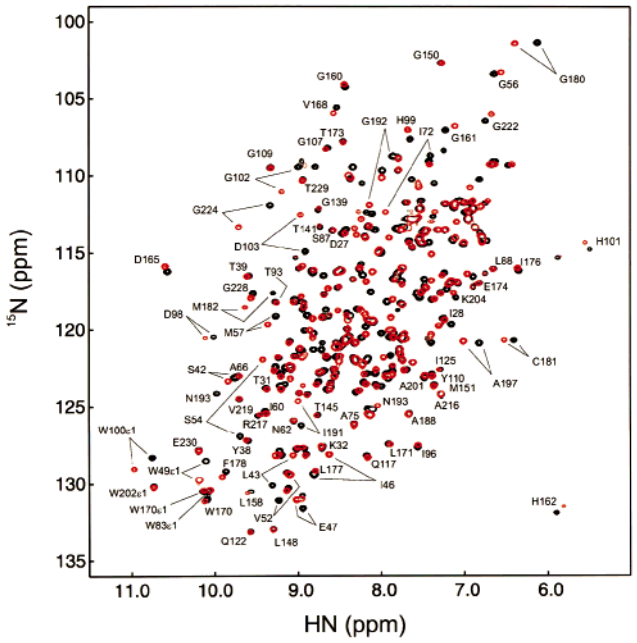

FIGURE 4: Superposition of the 750 MHz ^{15}N NHSQC spectrum of free metallo-β-lactamase (red) and the same protein bound to the inhibitor SB225666 (black). Both samples contained 0.9 mM protein in 10 mM HEPES buffer (pH 7.0) containing 10 mM $ZnCl_2$ and 0.01% NaN_3. An aliquot of DMSO was added to the free metallo-β-lactamase sample to allow for accurate comparison with the inhibitor-bound form, since the inhibitor is water-insoluble and was added to the sample in DMSO solution. The temperature was 22 °C.

CSI method and from the crystal structure are generally in very good agreement, but there are some discrepancies in the predicted lengths of the β-strands. The structure of the region between residues 42 and 55 differs among the published crystal structures (*11*−*13*); the consensus structure is a β-hairpin with variable position in relation to the remainder of the protein. Our NMR experiments indicate that residues 42−47 and 50−55 form β-structure (CSI > 0), while residues 48 and 49 are involved in a turn. A network of NOEs defines the connection between the β-strands for forming the β-hairpin. The NOEs that define the secondary structure of this region are shown schematically in Figure 3b.

The ^{13}C resonance assignments for the side chains are largely complete, but the difficulties of working with the overlapped proton NMR spectra of proteins as large as CcrA have slowed the assignment of side chain proton resonances. The only side chain proton resonances that have been assigned at this stage are the indole protons of the tryptophans, which were identified by using NOE connectivities to the sequentially assigned backbone NH resonances.

Effect of Inhibitor Binding on the NMR Spectrum. The addition of SB225666 to CcrA perturbs the backbone chemical shifts for a number of residues (Figure 4). Since many resonances in the ^{15}N HSQC spectrum shift dramatically upon inhibitor binding, assignments for the inhibitor-bound form were made independently without reference to those of the free form of the protein, using an independent set of NMR experiments. Figure 5 shows a plot of the changes in ^{1}HN, ^{15}N, and ^{13}Cα chemical shifts which occur upon inhibitor binding. Significant changes are observed in several regions of the protein sequence, which are generally localized in the three-dimensional structure in the vicinity of the zinc sites (Figure 6). Major chemical shift perturbations are observed for all three nuclei for residues in the "flexible flap" region (residues 44−52) and in the vicinity of residues 190−192. In addition, the indole NH cross-peaks of two of the tryptophans, W100 and W49, are substantially shifted (Figure 4).

Several resonances change their relaxation behavior upon inhibitor binding. Substantial changes occur for the backbone amides of W100 and I105. The cross-peak for the backbone amide group of W100 is not observed in the HSQC spectrum of the free enzyme, whereas it is present as a well-defined sharp resonance in the inhibitor-bound form. The resonances of I105 are significantly broadened in the absence of inhibitor, suggesting that motions on the chemical shift time scale are present. Consistent with the presence of motion, interresidue and intraresidue correlations are only partially observed for this spin system in triple-resonance experiments; unequivocal assignment of the I105 resonances could only be obtained through sequential HN−HN correlations in a ^{15}N NOESY-HSQC spectrum. In contrast, the I105 resonances are markedly stronger and sharper for the inhibitor-bound form, suggesting that a significant change in the mobility of the polypeptide in this region has accompanied the binding of SB225666. This is most likely an indication that these residues are involved in some kind of exchange process on the NMR time scale which is abrogated in the presence of bound inhibitor.

Despite these changes, it is apparent that the secondary structure of the loop is unchanged upon inhibitor binding, since the NOEs that define the β-hairpin (Figure 3b) are all present in the inhibitor-bound form as they are in the free form.

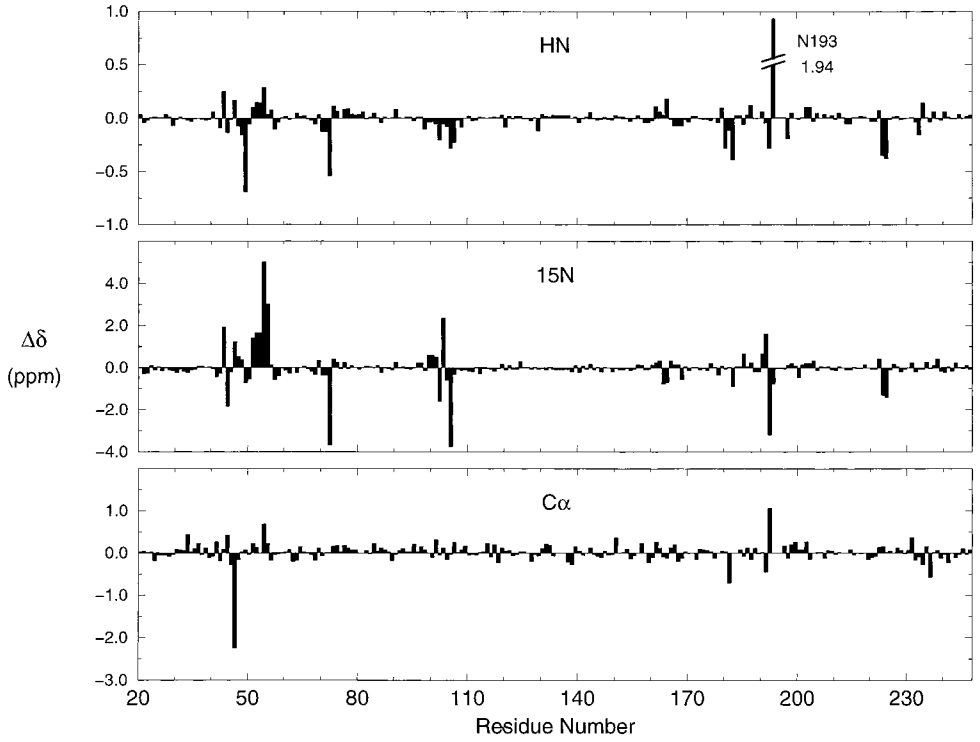

FIGURE 5: Changes in chemical shifts for NH, ^{15}N, and ^{13}Cα between the metallo-β-lactamase free and bound to the inhibitor SB225666. The chemical shift values for the free protein have been subtracted from those of the inhibitor-bound protein.

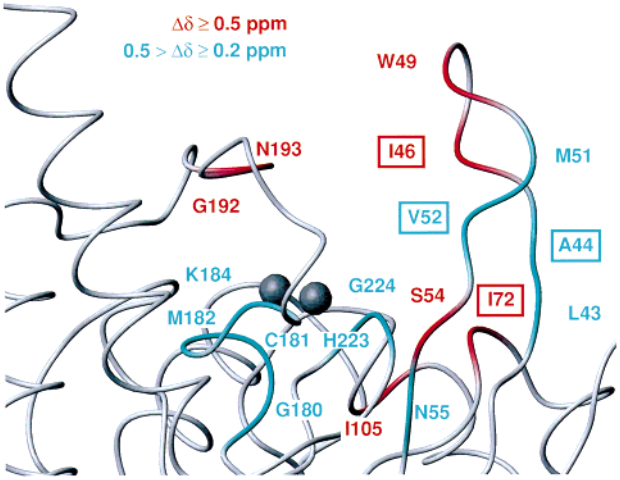

FIGURE 6: Location of residues with significantly perturbed amide proton and nitrogen resonances upon binding of SB225666, mapped onto the X-ray structure of the metallo-β-lactamase (*12*). The $\Delta\delta$ values are the absolute values of changes in amide proton and nitrogen chemical shifts and were calculated for each residue by adding the absolute value of the change in ^{1}H chemical shift to the absolute value of the ^{15}N chemical shift change, the latter divided by 10 to account for the difference in spectrometer frequency between ^{1}H and ^{15}N.

Heteronuclear NOE Measurements. The heteronuclear ^{1}H−^{15}N NOE gives a qualitative measure of the mobility of the polypeptide backbone on a sub-nanosecond time scale at local sites throughout the protein. Figure 7 shows the heteronuclear NOEs for the backbone amides and for the indole NH of the tryptophan residues, in the free and inhibitor-bound states of the metallo-β-lactamase. The large uncertainties in the NOE data are a result of the necessity for using low sample concentrations to minimize the likelihood of unfolded and/or aggregated protein in the solution. Within these experimental errors, the NOEs appear to be

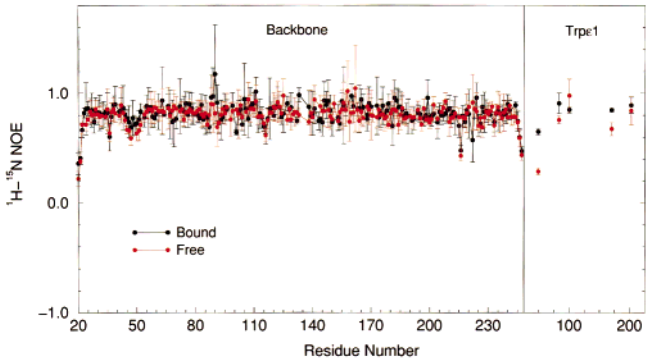

FIGURE 7: Plot of the backbone ^{1}H−^{15}N NOE measured at 600 MHz at each site in the protein. The protein concentration was 250 μM in each case. The temperature was 22 °C. Values for the tryptophan indole NH are shown in a separate section at the right of the figure.

very similar over most of the backbone for the free and bound forms.

The average value of the backbone ^{1}H−^{15}N NOE excluding the three residues at the N- and C-termini is 0.82 ± 0.10 for the inhibitor-bound form of the protein and 0.81 ± 0.12 for the free form. The tryptophan side chains in general exhibit high heteronuclear NOEs and very little difference between free and bound forms, consistent with their presence in the hydrophobic core of the protein. The exception is Trp49, which is highly mobile in the free form, with a heteronuclear NOE value of 0.28. The inhibitor-bound form exhibits much less mobility, with a value of 0.6. The backbone heteronuclear NOEs for the region between residues 40 and 50 are consistently lower than the average for both the free and bound forms of the protein, indicating an increased flexibility on the nanosecond time scale. However, the extent of the decrease is not so great as to indicate that this region is unfolded. This is consistent with

the NMR chemical shifts and resonance line widths in this region, which indicate that the region forms an integral part of the protein. While the NOEs in this region suggest some increase in flexibility over that of the protein as a whole, this increase is typical for loops in proteins and occurs also, for example, in the region between residues 113 and 118 (Figure 7). We conclude that the evidence of motion in this loop inferred from the crystal structure temperature factors does not reflect extensive motion on a picosecond to nanosecond time scale for the backbone of the region of residues 44−52 in solution. These results do not rule out segmental motion of the entire β-hairpin as a result of the binding of molecules of different sizes and shapes. Segmental motion of this type can be identified by the presence of exchange terms in a full dynamics analysis. These studies are in progress, but are beyond the scope of this paper.

DISCUSSION

Stabilization of the Metal-Binding Monomer. An important practical consideration for work with CcrA is the irreversible aggregation that occurs when zinc is removed or depleted from the enzyme. The original crystal structure of the homologous enzyme from *Bacillus cereus* (*31*) exhibited only a single bound zinc ion. The presence of two zinc ions in the CcrA enzyme from *B. fragilis* was confirmed both by the X-ray crystal structures (*11*−*13*, *32*) and by careful biochemical studies (*10*). It appears that Zn can be replaced by Co or Cd with retention of activity, but Hg substitution causes inactivation of the enzyme, due to changes in the metal-binding site (*32*). A higher-resolution crystal structure of the *B. cereus* enzyme (*33*) also confirmed that there are two zinc ions in this molecule, although the binding of one of the two zinc ions appears to be weak and the local structure different from that of the *B. fragilis* enzyme. We have found that the integrity of the zinc site is a prerequisite for stability of the *B. fragilis* enzyme in solution. In the presence of reagents which have a measurable tendency to remove zinc from the enzyme, the protein forms soluble, partly unfolded aggregated forms, and this behavior is intensified at higher concentrations of, for example, EDTA or phosphate. The increased stability of the protein as a monomer in solution upon inhibitor binding also suggests that binding of inhibitor (or substrate) stabilizes the zinc site. Part of this stabilization may be simply due to the lower solvent accessibility of the zinc ions.

Aspects of the architecture of the metallo-β-lactamase show adaptations of the protein structure for the stabilization of the zinc site. The crystal structure (*11*) suggests that the Y157 OH is well-positioned to interact with T164 CO (Figure 8). The residue that follows T164 is the buried aspartate D165, which governs the correct orientation for metal binding by three ligands (H99, H101, and H162) through an interaction between its carboxylate group and the backbone amide of W100 (*11*). Local structure stabilization can also be directly inferred from the NMR experiments. For both free and bound CcrA, the NH resonance of G159 is shifted 3.23 ppm upfield of the random coil chemical shift for a glycine (*34*). The predicted chemical shift perturbation attributed to aromatic ring currents is approximately 2.1 ppm (*35*), and suggests that the remaining upfield contribution comes from some other source. One possibility involves the formation of an amide−aromatic "hydrogen bond" interaction between G159 NH and the Y157 side chain, which is certainly consistent with their close approach in the X-ray crystal structure (*11*) (Figure 8). Close approach of a glycine amide proton to an aromatic ring in the $i - 2$ position was first noted in peptide studies (*36*, *37*). Recent studies of the immunophilin-like domain of FKBP59 (*38*) and *Fusarium solani pisi* cutinase (*39*) have also attributed similar high-field amide proton chemical shifts to amide−aromatic hydrogen bonds.

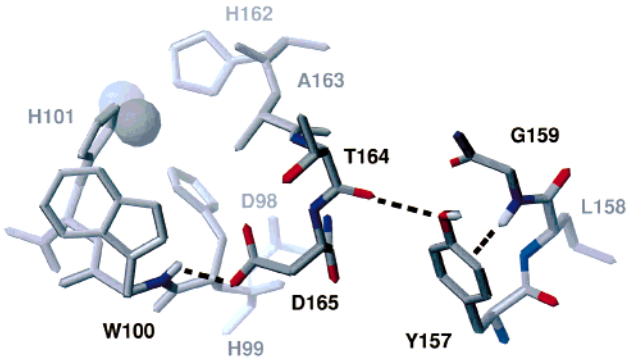

FIGURE 8: Portions of the X-ray crystal structure of the metallo-β-lactamase (*12*) showing the close approach of residues G159, Y157, and T164.

Inhibitor Binding Site. The inhibitor SB225666 exhibits many structural similarities to the β-lactam antibiotic ampicillin (Figure 2). Both possess a carboxy-dimethylthiazolidine moiety, but the closed β-lactam ring in ampicillin is replaced with an open mercapto derivative in SB225666. The changes in chemical shifts upon binding of inhibitor (Figures 4 and 5) indicate that the overall three-dimensional structure of the protein is unchanged, but a highly localized region abutting the zinc binding site, including β-hairpin residues 44−52, is significantly affected (Figure 6). According to the model of Herzberg and co-workers (*11*), the β-side chain substituents of commonly hydrolyzed antibiotics such as ampicillin and ceftazidime can be well-accommodated by a hydrophobic pocket formed by residues A44, I46, V52, and I72. SB225666 possesses a similar moiety in its β-position, and residues I46, W49, S54, and I72 all exhibit significant perturbations upon inhibitor binding (Figure 5). The most significant perturbation upon inhibitor binding is experienced by N193, with K184 affected to a lesser extent. These chemical shift changes suggest that SB225666 binds in a position similar to that thought to be occupied by β-lactam antibiotics.

Since SB225666 has a free sulfhydryl group, it is possible that it is bound to the protein through a disulfide-like interaction with one of the free cysteine side chains in the vicinity of the zinc-binding site (C104 and C181). The Cα and Cβ chemical shifts of the cysteine residues in the vicinity of the active site in the presence and absence of inhibitor exhibit no significant perturbation, remaining characteristic of reduced SH. These results indicate that disulfide bond formation between SB225666 and either of the cysteines is not an important factor in inhibitor binding.

Changes in a Crucial Stabilizing Residue. The side chain carboxylate of the buried residue D69 interacts with groups involved in correctly orienting the three zinc ligands, H99, C181, and D103 (*11*), and it has been suggested that the strained conformation adopted by D69 ($\phi = 81°$ and $\psi = 144°$) may be relevant to the function of the enzyme.

Addition of the inhibitor results in a significant shift of the D69 Cβ resonance (0.35 ppm), whereas all other backbone nuclei of the same residue are relatively unaffected. As Cβ nuclei are affected predominantly by changes in secondary structure, the change in the chemical shift of D69 Cβ may indicate that a highly specific conformational change accompanies substrate or inhibitor binding. Interestingly, the NMR signature of a positive ϕ, a high-intensity $d_{N\alpha}(i,i)$ NOE cross-peak (*40*), is absent from the NOESY spectra of both free and bound enzyme, raising the question of the possibility of a local difference in the conformation of this residue between crystal and solution. In the crystal structure, a Na^+ ion contacts the D69 carboxyl group, only 8 Å from the nearest Zn^{2+}. The less strained negative ϕ value for D69 in the NMR spectra may be linked to the absence of Na^+ in the NMR buffer.

Structure of the Active-Site β-Hairpin Loop. The crystal structures of CcrA indicate that residues 44−52 are highly variable. It is usual to observe that loop regions of a protein have greater apparent flexibility in solution than in the crystal. However, in this case, we do not find evidence for serious conformational heterogeneity in solution for the loop of residues 44−52 in the absence of inhibitor. Evidence for well-formed β-structure was recognizable (Figure 3). In particular, NOE connectivities linking backbone amide protons G50 and G48, as well as an NH−Hα connectivity between G50 and E47, were identified, indicating the presence of a β-hairpin structure consistent with that inferred from crystal structures (*12*, *13*). In addition, resonances with regular size and shape were observed in the NMR spectrum for residues in the loop, indicating that the loop does not differ greatly in its relaxation behavior from the remainder of the protein.

Effects of Inhibitor Binding on the Active-Site β-Hairpin Loop. The chemical shift changes induced by the addition of SB225666 (Figure 5) are an indication that the β-hairpin loop region (residues 44−52) plays a role in binding of substrates. Major changes in the backbone structure of the loop itself upon binding of inhibitor are ruled out, since CSI and $^1H-^1H$ NOE data indicate that the overall β-hairpin structure is retained in the bound form. A small but consistent increase in the backbone $^{15}N-^1H$ heteronuclear NOE value is observed in this region upon inhibitor binding (Figure 7). These results suggest that the position of the loop is changed upon inhibitor binding, accompanied by a small decrease in the local backbone mobility.

The most significant changes in NMR chemical shifts and dynamics are experienced by the side chains in the region of the metal site. The side chain amide protons for tryptophans W49 and W100 experience significant shifts for both ^{15}N and ^1H nuclei upon binding of SB225666 (Figure 4), and a substantial change is observed for the heteronuclear NOE of the side chain of W49 (Figure 7). This suggests that the motion of the W49 side chain is damped upon binding of the inhibitor, and approaches that of the backbone in the bound form. This tryptophan forms part of the terminal β-turn in the β-hairpin loop, an unusual position for such a bulky residue, since it virtually guarantees that the side chain will be exposed to solvent. However, it is clear that it makes intimate contact with the inhibitor in the complex, suggesting that it plays a crucial role in recruiting and stabilizing ligands. The overall structure of the hairpin loop would be ideally suited to behaving as a "fishing rod", allowing the binding of a wide range of different substrate molecules in a binding pocket of variable width and depth. The fact that this pocket is lined with hydrophobic residues whose backbone resonances are perturbed upon binding of inhibitor (Figure 6) lends further support to this view. These observations suggest that the loop of residues 44−52 may function to provide a rather plastic hydrophobic pocket where the aromatic moiety of the substrate can be securely bound, rather than, as has been suggested (*13*), as a means of locking the substrate in place. Plasticity of this kind is consistent with the wide substrate specificity of the CcrA enzyme.

ACKNOWLEDGMENT

We thank Dr. Beth A. Rasmussen for providing the original *B. fragilis* metallo-β-lactamase (ccrA) clone, Smith-Kline Beecham for providing the inhibitor SB225666, and Dr. Zhigang Wang for valuable discussions on the preparation of the protein.

SUPPORTING INFORMATION AVAILABLE

A table describing in detail the NMR experiments used for the assignment of the resonances of the free and inhibitor-bound metallo-β-lactamase. This material is available free of charge via the Internet at http://pubs.acs.org.

REFERENCES

1. Hughes, J. M., and Tenover, F. C. (1997) *Clin. Infect. Dis. 24*, S131−S135.
2. Knowles, J. R. (1985) *Acc. Chem. Res. 18*, 97−104.
3. Bush, K., Jacoby, G. A., and Medeiros, A. A. (1995) *Antimicrob. Agents Chemother. 39*, 1211−1233.
4. Bush, K. (1989) *Antimicrob. Agents Chemother. 33*, 271−276.
5. Payne, D. J., Bateson, J. H., Gasson, B. C., Khushi, T., Proctor, D., Pearson, S. C., and Reid, R. (1997) *FEMS Microbiol. Lett. 157*, 171−175.
6. Bandoh, K., Muto, Y., Watanabe, K., Katoh, N., and Ueno, K. (1991) *Antimicrob. Agents Chemother. 35*, 371−372.
7. Watanabe, M., Iyobe, S., Inoue, M., and Mitsuhashi, S. (1991) *Antimicrob. Agents Chemother. 35*, 147−151.
8. Payne, D. J. (1993) *J. Med. Microbiol. 39*, 93−99.
9. Cuchural, G. J., Malamy, M. H., and Tally, F. P. (1986) *Antimicrob. Agents Chemother. 30*, 645−648.
10. Crowder, M. W., Wang, Z., Franklin, S., Zovinka, E., Que, L., Jr., and Benkovic, S. J. (1996) *Biochemistry 35*, 12126−12132.
11. Concha, N. O., Rasmussen, B. A., Bush, K., and Herzberg, O. (1996) *Structure 4*, 823−836.
12. Carfi, A., Duée, E., Paul-Soto, R., Galleni, M., Frère, J.-M., and Dideberg, O. (1998) *Acta Crystallogr., Sect. D 54*, 47−57.
13. Fitzgerald, P. M., Wu, J. K., and Toney, J. H. (1998) *Biochemistry 37*, 6791−6800.
14. Yang, Y., Rasmussen, B. A., and Bush, K. (1992) *Antimicrob. Agents Chemother. 36*, 1155−1157.
15. Neidhardt, F. C., Bloch, P. L., and Smith, D. F. (1974) *J. Bacteriol. 119*, 736−747.
16. Venters, R. A., Huang, C.-C., Farmer, B. T. I., Trolard, R., Spicer, L. D., and Fierke, C. A. (1995) *J. Biomol. NMR 5*, 339−344.
17. Glasoe, P. K., and Long, F. A. (1960) *J. Chem. Phys. 64*, 188−190.
18. Sambrook, J., Fritsch, E. F., and Maniatis, T. (1989) in *Molecular Cloning. A Laboratory Manual*, Cold Spring Harbor Laboratory Press, Cold Spring Harbor, NY.
19. Rasmussen, B. A., Gluzman, Y., and Tally, F. P. (1990) *Antimicrob. Agents Chemother. 34*, 1590−1592.

20. Kay, L. E., Keifer, P., and Saarinen, T. (1992) *J. Am. Chem. Soc. 114*, 10663−10665.
21. Muhandiram, D. R., and Kay, L. E. (1994) *J. Magn. Reson., Ser. B 103*, 203−216.
22. Marion, D., Ikura, M., Tschudin, R., and Bax, A. (1989) *J. Magn. Reson. 85*, 393−399.
23. Grzesiek, S., and Bax, A. (1993) *J. Am. Chem. Soc. 115*, 12593−12594.
24. Delaglio, F., Grzesiek, S., Vuister, G. W., Guang, Z., Pfeifer, J., and Bax, A. (1995) *J. Biomol. NMR 6*, 277−293.
25. Johnson, B. A., and Blevins, R. A. (1994) *J. Chem. Phys. 29*, 1012−1014.
26. Wishart, D. S., Bigam, C. G., Yao, J., Abildgaard, F., Dyson, H. J., Oldfield, E., Markley, J. L., and Sykes, B. D. (1995) *J. Biomol. NMR 6*, 135−140.
27. Scrofani, S. D. B., Wright, P. E., and Dyson, H. J. (1998) *Protein Sci. 7*, 2476−2479.
28. Scrofani, S. D. B., Wright, P. E., and Dyson, H. J. (1998) *J. Biomol. NMR 12*, 201−202.
29. Wishart, D. S., and Sykes, B. D. (1994) *J. Biomol. NMR 4*, 171−180.
30. Laskowski, R. A., MacArthur, M. W., Moss, D. S., and Thornton, J. M. (1993) *J. Appl. Crystallogr. 26*, 283−291.
31. Carfi, A., Pares, S., Duée, E., Galleni, M., Duez, C., Frére, J. M., and Dideberg, O. (1995) *EMBO J. 14*, 4914−4921.
32. Concha, N. O., Rasmussen, B. A., Bush, K., and Herzberg, O. (1997) *Protein Sci. 6*, 2671−2676.
33. Fabiane, S. M., Sohi, M. K., Wan, T., Payne, D. J., Bateson, J. H., Mitchell, T., and Sutton, B. J. (1998) *Biochemistry 37*, 12404−12411.
34. Wishart, D. S., Bigam, C. G., Holm, A., Hodges, R. S., and Sykes, B. D. (1995) *J. Biomol. NMR 5*, 67−81.
35. Johnson, C. E., and Bovey, F. A. (1958) *J. Chem. Phys. 29*, 1012−1014.
36. Dyson, H. J., Merutka, G., Waltho, J. P., Lerner, R. A., and Wright, P. E. (1992) *J. Mol. Biol. 226*, 795−817.
37. Kemmink, J., van Mierlo, C. P. M., Scheek, R. M., and Creighton, T. E. (1993) *J. Mol. Biol. 230*, 312−322.
38. Craescu, C. T., Rouvière, N., Popescu, A., Cerpolini, E., Lebeau, M. C., Baulieu, E. E., and Mispelter, J. (1996) *Biochemistry 35*, 11045−11052.
39. Prompers, J. J., Groenewegen, A., Van Schaik, R. C., Pepermans, H. A. M., and Hilbers, C. W. (1997) *Protein Sci. 6*, 2375−2384.
40. Kline, A. D., Braun, W., and Wüthrich, K. (1988) *J. Mol. Biol. 204*, 675−724.

BI990986T